



Influence of Using Straight and Twisted Elliptical Section Heater Tubes on Stirling Engine Performance

Received 18 July 2022; Revised 12 September 2022; Accepted 13 September 2022

Ahmed Abdelnaby¹
Saleh Abo-Elfadl²
O. Hassan[†]
Ibrahim, A. M.[‡]

Keywords

Stirling engine, Heater tubes, Elliptical, Twist ratio, Thermal efficiency

Abstract

The heat transfer area of the heater tubes is a significant factor that deeply affects output power and thermal efficiency in Stirling engines. Alpha-type Stirling engine is concerned in this study. Circular section, elliptical section, twisted elliptical section tubes having twist ratios of 2, 3 and 4 are used as heater designs. 3D simulation model using SST K- ω turbulent model is used for simulating airflow through the hot cylinder, heater tubes, regenerator, cooler, and cold cylinder of the Stirling engine, during a complete engine cycle. The results showed that the elliptical section tubes are better than the circular section tubes. The maximum input energy rate, output work and thermal efficiency are achieved by using elliptical section with twist ratio of 2. These values are 4245.87 W, 1225.34 W and 29.55%, respectively with percentage increments of 5.2%, 7.47% and 3.76%, respectively relative to the circular section heater tubes.

1. Introduction

Stirling engine is a heat engine operating by cyclic compression and expansion of air or other gases (hydrogen or helium) as a working fluid at different temperature levels that converts the thermal energy to mechanical work. Robert Stirling in Scotland invented it in 1816, 80 years before the invention of the diesel engine. It is light weight and reasonably compact. It is also significantly safer and more efficient than fuel engines such as Gasoline and Diesel engines at the same temperature levels of added and rejected thermal energy (TH and TL).

¹ Assiut Oil Refining Company (ASORC)-Assiut, Egypt. ahmedahmed.eng19918@gmail.com

² Assoc. Professor, Dept. of Mechanical Power Eng., Assiut University, Assiut, Egypt. salehaboelfadl2@gmail.com

³ Assist. Professor, Dep. of Mechanical Power Eng., Assiut University, Assiut, Egypt. othman.hassan@eng.aun.edu.eg

⁴ Emeritus Professor, Dep. of Mechanical Power Eng., Assiut University, Assiut, Egypt. abdibr@aun.edu.eg

Stirling engine components are 40% less than that of the internal combustion engine. Besides conventional energy sources, it can operate with renewable energy fuels such as Biogas and Biomass fuels. Moreover, recent designs of Stirling engines can operate with solar energy as a green renewable energy source. Stirling engine efficiency is still low; therefore, more research work is still needed. Many researchers attempted to increase engine efficiency through the using of different working fluids types and different filling pressures, different porous media types and porosity ratios, different heater tubes design parameters (number, diameter and length).

Lloyd [1] developed a low-temperature differential Stirling engine that generated electric power from heat sources such as wasted hot water. The engine was simulated numerically using SAGETTM code. The results showed that the wasted hot water of industrial processes can be used as a heat source with this engine type. Coal-bed methane (CBM) fuel can be used as an energy source for Stirling engine. Bao-sheng et al [2] constructed CBM burner and fastened the heater tubes of the Stirling engine in the burner. They found that, despite the fuel flame instability, the porous burner achieves reasonable stability, enabling the Stirling engine to run satisfactorily. Cheng and Yu [3] developed a numerical model for a beta-type Stirling engine driven with a rhombic mechanism considering the non-isothermal effects. The results showed that by adjusting the regenerative gap, the distance between the two rhombic mechanism gears, and the heat source temperature, the engine performance could be improved. A thermodynamic model through the compression and expansion volumes of Stirling engine is carried out by Tarawneh et al [4]. The obtained results showed that the lowered performance of the real Stirling engine was associated with some deficiencies such as the non-ideal regeneration, the gas leakage, and the significant friction related to the flowing agent through the heat exchangers. With the aid of experimental data, Ahmadi et al [5] modelled the distribution of output torque and power of the Stirling engine using method of data handling (GMDH) approach. The results showed that the method has a high level of robustness and integrity for determining output power and torque. It can help, reliability, energy experts and designers for improving Stirling engine performance. Chmielewski et al [6] developed a thermodynamic analysis for a micro-cogeneration system consisting of the internal combustion engine with a single-action alpha-type Stirling engine and electrical thermo-generators. They found that the increase of gas pressure, the heat source temperature, and the regenerator's heat efficiency increases the efficiency of the micro-cogeneration system. Different thermodynamic simulation models are investigated by Hoegel [7] for examining Stirling engine performance. The results showed that the non-isothermal approach is reasonably accurate for the simulation. In addition, that the phase angle, regenerator porosity, and temperature levels are the most sensitive parameters for power and efficiency. The temperature distribution and temperature gradient over Stirling engine components are visualized through the using of Schlieren technique by Alvarez-Herrera et al [8]. The obtained results gave important information about the heat transfer mechanism, energy dissipation from the real engine. For improving the heat transfer process through the outer surfaces of heater tubes, Ke Li et al [9] studied the use of liquid metal of Sodium–potassium alloy (NaK) flowing through a passage surrounding the heater tubes. They found that the temperature difference between the NaK and the working fluid is significantly reduced due to the increase in heat transfer coefficient. Another attempt for increasing the heat transfer rate in the heater tubes is studied numerically by Karabulut et al [10]. They suggested a heater design of parallel circular section tubes included in square section ducts. The hot gases pass through the four gaps between the square and the included circle sections and the working fluid passes through the circular tubes. They found that the suggested design increases Nusselt number of the working fluid and hence the heat transfer

coefficient. The influence of the heater tube diameter on the engine performance is studied by Thom bare et al [11] numerically. They constructed a CFD simulation model for the Stirling engine heater with tube of 3 mm, 4 mm, and 5 mm diameters. The results showed that the heat transferred through the heater decreased with the increase of tube inner diameter. A heater made of ceramic material is designed by Akazawa et al [12] for improving the heat transfer rate in Stirling engine. They examined the design experimentally and the results showed that the ceramic material increases the heat transfer rate and the thermal efficiency.

The regenerator design has a significant effect on Stirling engine performance. Therefore, many researchers focused their work on the regenerator materials dimensions and porosity ratio. Kumar and Kuzhivel [13] investigated the regenerator performance numerically under steady and unsteady flow conditions. They used different sizes of stainless-steel wire meshes. They found that small size wire meshes achieved better performance than large size wire meshes. Regenerator composed of different sizes of wire meshes is examined by Andersen et al [14] numerically. The suggested regenerator design had three matrix sections which were different in wires' thickness. The results showed that this design improved the engine efficiency from 32.9 % to 33.2 %, with a 3 % decrease in output power relative to thin wire meshes regenerator. The effect of the regenerator wires material is investigated experimentally by Gheith et al [15] in gamma-type Stirling engine. They used different materials such as stainless steel, copper, aluminium, and Monel 400. Experimental results showed that Monel 400 and stainless-steel regenerators presented an acceptable thermal efficiency and did not oxidize.

In spite of the above studies on the heat transfer characteristics development inside Stirling engine, more attempts and modifications are still required for increasing the output power and thermal efficiency of the engine.

In this study, new design of elliptical section heater tubes is suggested to increase the heat transfer area between the heater walls and working fluid. Straight and twisted elliptical section tubes are examined. Three elliptical twisted tubes with twist ratios of two, three, and four are used. The twisted tubes designs increase the path length of the working fluid and tube surface area which enhances the heat transfer process, output power, and thermal efficiency. The output results are compared to circular section heater tubes.

2. Engine simulation model

For examining the heater tubes designs, an alpha-type Stirling engine is constructed using Gambit program. Firstly, conventional circular section heater tubes are constructed on the engine (reference case). Secondly, straight and three twisted ratios elliptical tubes are constructed also. Each of the previous five designs of heater tubes is merged with the engine separately forming five engine designs. The following subtitles will describe the engine geometry, heater geometry, numerical model, boundary and operating conditions besides the model validation.

2.1. Engine geometry and specifications

Figure 1 illustrates a schematic and 3D view of the engine and table 1 illustrates the engine specifications. The engine dimensions are considered according to gamma-type Stirling engine ST05G-CNC [16] and [17] with changing the hot cylinder displacer to power piston to convert it from gamma to alpha type. The connecting duct (circular tube in the original design in [16] and [17]) is replaced by rectangular duct having cross of 53 mm*10 mm (Part

4 in Fig. 1). The dimensions of the duct are selected to achieve the same cooling effect of the original design at cooling temperature of 300 K. Therefore, the connecting duct will be called “the cooler” in this work. In addition, the regenerator porous media consists of a stacked wired array. Each wire diameter equals 55 μm and is made from a stainless-steel material with a porosity ratio of 90 %. The heater consists of 20 tubes.

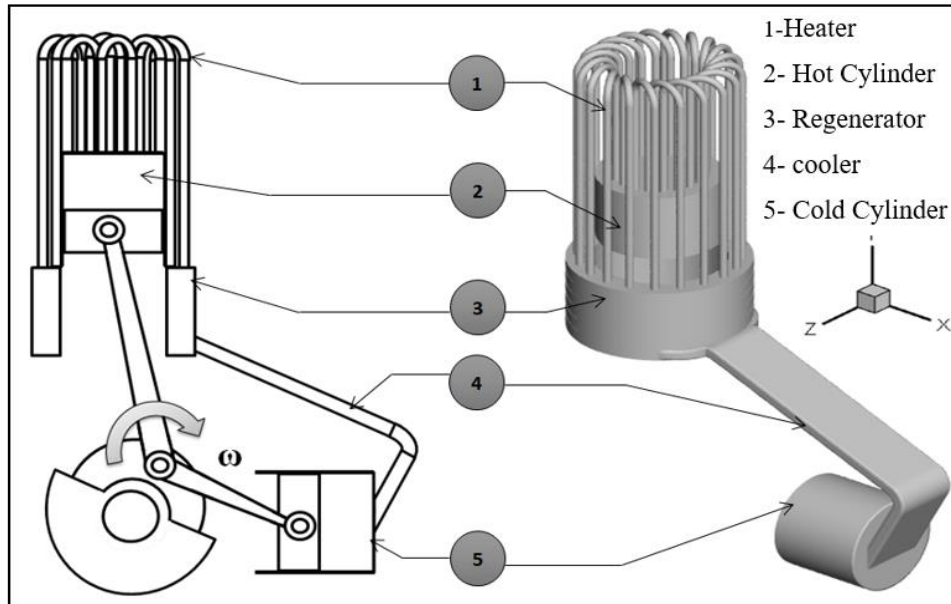


Fig. 1 Schematic and 3D view of the engine

Table 1. The engine specifications

| | | |
|----|---|---------------------|
| 1 | Hot cylinder bore | 92 mm |
| 2 | Cold cylinder bore | 85 mm |
| 3 | Heater tube cross-section area | 28.26 mm^2 |
| 4 | Cooler | 53*10 mm^2 |
| 5 | Regenerator (porous media) porosity | 90% |
| 6 | Crank radius | 37.5 mm |
| 7 | Connecting rod length | 150 mm |
| 8 | Engine speed | 500 rpm |
| 9 | Initial filling gage pressure | 10 bars |
| 10 | The shift Phase angle between the two cylinders | 90 deg. |
| 11 | Compression ratio | 1.0267 |
| 12 | Working fluid | air |

2.2. Heater's geometries

Five designs of the heater tubes are considered in this work. The different designs of the tubes have the same cross section area and volume to avoid their variation effects on the engine performance. The first design is convectional circular section tubes. The second is elliptical section tubes. The third, fourth and fifth are elliptical section tubes with twist ratios (TR) of two (2TR), three (3TR) and four (4TR), respectively. Figure 2 and table 2 illustrate 3D view and the dimensions of the circular section heater tubes.

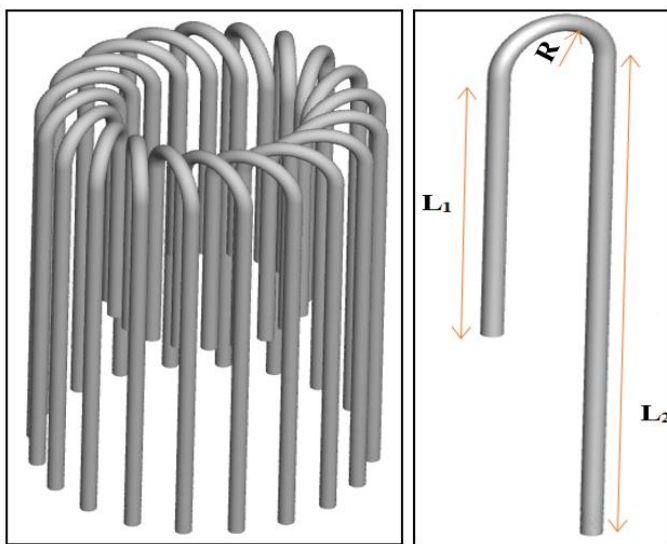


Fig. 2. 3D view of the circular section heater tubes

Table 1. The dimensions of each tube

| Parameter | Total length | L_1 | R | L_2 | diameter |
|--------------------|--------------|-------|------|-------|----------|
| dimensions in (mm) | 332 | 98 | 16.2 | 183 | 6 |

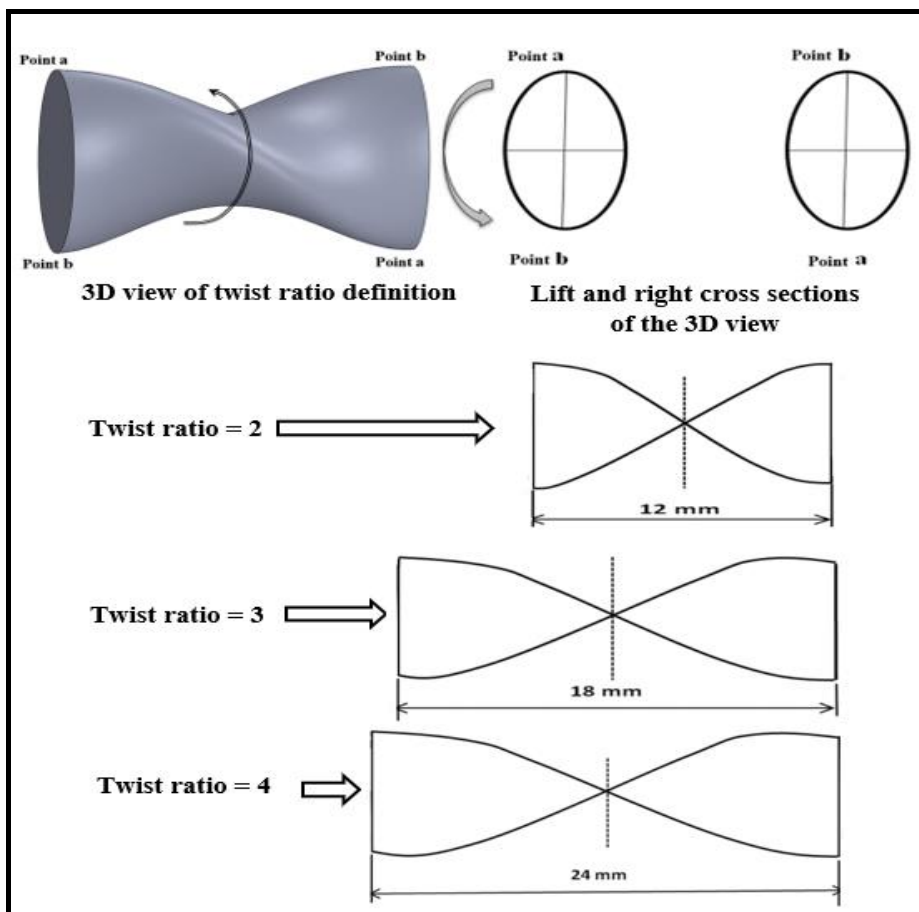
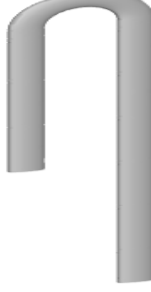
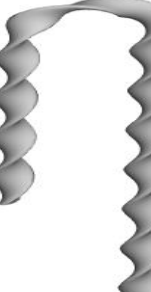


Fig. 3. Twist ratio definition and the three selected ratios

The twist ratio (TR) is defined as “*the ratio of the linear distance of the tube for 180° rotation angle about its axis to the diameter of the tube*”. Figure 3 illustrates twist ratio definition and table 3 illustrates 3D views of the five heater tubes, their cross sections, total surface area and hydraulic diameter. The five designs have cross section area of 28.28 mm^2 .

Twisting the elliptical tubes increases the surface area. The total surface areas of the heater tubes are 0.125, 0.144, 0.16, 0.165 and 0.179 m² for circular section, elliptical, elliptical 4TR, elliptical 3TR and elliptical 4TR respectively.

Table 3. 3D view of the heater tubes and their sections.

| Circular | Elliptical | Elliptical 4TR | Elliptical 3TR | Elliptical 2TR |
|---|---|---|--|---|
|  |  |  |  |  |
| A _s =0.125 m ² | A _s =0.144 m ² | A _s =0.16 m ² | A _s =0.165 m ² | A _s =0.179 m ² |
| D _h =6 mm | D _h =4.88 mm | D _h =4.88 mm | D _h =4.88 mm | D _h =4.88 mm |

2.3. Simulation Model

The three-dimensional flow characteristics in the cylinder are investigated by solving the continuity, momentum, and energy equations in conjunction with the equations of the turbulence model. In the present work, the shear stress transport turbulence model (SST k- ω) is used to simulate the turbulent flow in the engine as it achieved good results in many studies in Stirling engines [18], [19] and [20].

2.3.1. Governing equations

Continuity equation:

$$\frac{\partial \rho}{\partial t} + \frac{\partial}{\partial x_i} (\rho u_i) = 0 \quad (1)$$

Momentum equation:

$$\frac{\partial}{\partial t} (\rho u_i) + \frac{\partial}{\partial x_j} (\rho u_i u_j) = - \frac{\partial p}{\partial x_i} + \frac{\partial}{\partial x_j} \left[\mu_{eff} \left(\frac{\partial u_i}{\partial x_j} + \frac{\partial u_j}{\partial x_i} - \frac{2}{3} \delta_{ij} \frac{\partial u_i}{\partial x_i} \right) - \frac{2}{3} \delta_{ij} \rho k \right] \quad (2)$$

Energy equation:

$$\frac{\partial}{\partial t} (\rho e_o) + \frac{\partial}{\partial x_i} [u_i (\rho e_o + p)] = \frac{\partial}{\partial x_j} \left(k_{eff} \frac{\partial T}{\partial x_j} + u_i (\tau_{ij})_{eff} \right) \quad (3)$$

Where k_{eff} is the effective thermal conductivity, and $(\tau_{ij})_{eff}$ is the derivative stress tensor, which is defined as:

$$(\tau_{ij})_{eff} = \mu_{eff} \left(\frac{\partial u_j}{\partial x_i} + \frac{\partial u_i}{\partial x_j} \right) - \frac{2}{3} \mu_{eff} \frac{\partial u_k}{\partial x_k} \delta_{ij} \quad (4)$$

$$\mu_{eff} = \mu_L + \mu_t \quad (5)$$

$$e_o = e + \frac{u^2}{2} \quad (6)$$

The two equations of the SST k- ω model are described as follows:

1- Turbulent kinetic energy equation:

$$\frac{\partial}{\partial t} (\rho k) + \frac{\partial}{\partial x_i} (\rho k u_i) = \frac{\partial}{\partial x_i} \left(\Gamma_k \frac{\partial k}{\partial x_i} \right) + \tilde{G}_k - Y_k \quad (7)$$

2- Specific dissipation rate equation:

$$\frac{\partial}{\partial t} (\rho \omega) + \frac{\partial}{\partial x_i} (\rho \omega u_i) = \frac{\partial}{\partial x_i} \left(\Gamma_\omega \frac{\partial \omega}{\partial x_i} \right) + \tilde{G}_\omega - Y_\omega + D_\omega \quad (8)$$

where Γ_k and Γ_ω represent the effective diffusivities of turbulence kinetic energy k , and the specific dissipation rate of energy ω , respectively. \tilde{G}_k and \tilde{G}_ω represent the generation of k and ω , respectively. Y_k and Y_ω represent the dissipation of k and ω , respectively. D_ω represents the cross-diffusion term. These terms are illustrated in ANSYS FLUENT-16 user guide. The effective thermal conductivity of the porous media, K_{eff} is computed by Eqn. (9) from ANSYS FLUENT User's Guide [21]:

$$K_{eff} = \gamma K_f + (1-\gamma) K_s \quad (9)$$

The following equations compute the Viscous and Inertial resistance coefficients in the regenerator porous media [21]:

1-Viscous resistance coefficients = $1/\dot{\alpha}$

$$\dot{\alpha} = \frac{d_w^2}{150} \frac{\gamma^3}{(1-\gamma)^2} \quad (10)$$

2-Inertial resistance coefficients = \dot{C}_2

$$\dot{C}_2 = \frac{3.5}{d_w} \frac{(1-\gamma)}{\gamma^3} \quad (11)$$

The Interfacial area density of porous media zone can be calculated from:

$$A_i = \frac{\text{Area heat transfer}}{\text{volume of porous media zone}} = \frac{4*\gamma}{D_h} \quad (12)$$

Where: Hydraulic diameter (D_h) of porous media zone can be calculated from the following equation:

$$D_{\hat{h}} = \frac{\gamma}{1-\gamma} d_w \quad (13)$$

The inter-phase Nusselt Number Nu_i correlation for wired mesh porous media is calculated as [22]:

$$Nu_i = 1.91 + 0.17 * Re_i^{0.8} \quad (14)$$

Where Re_i is the interspatial Reynolds number and expressed by equation (7):

$$Re_i = \frac{\rho_f * u_{max} * D_{\hat{h}}}{\mu_f} \quad (15)$$

And ρ_f is working fluid density computed by ideal gas equation

$$\rho_f = \frac{P_i}{R * T_m} \quad (16)$$

The governing equations are solved through all engine components as transient state by ANSYS FLUENT-16.

2.3.2. Boundary conditions

The wall temperatures of heater tubes and the hot cylinder are assumed to be a constant having value of 900 K. Also, the wall temperatures of the cold cylinder and the cooler are assumed to be a constant with a value of 300 K. The walls of other components are assumed to be adiabatic. During the engine cycle, the hot and cold pistons are considered movable boundaries. Their motions are programmed by C++ and imported in ANSYS FLUENT-16 as a UDF file. The initial position of the hot cylinder piston is at its BDC as shown in Fig. 4. At this position, the cold cylinder piston position is away from its BDC by a 31 mm distance.

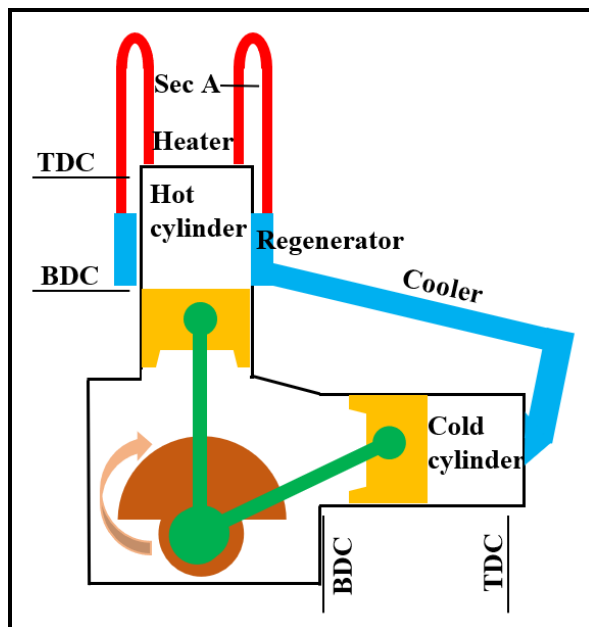


Fig. 4. The first position of the engine pistons

The engine is operated at 500 rpm with initial filling pressure of 10 bar. The time step of calculation is 0.0003333 seconds which corresponds to one-degree crank angle at the mentioned rotational speed.

2.3.3. Mesh size and validation

To select the best grid size for heater tubes' zone, which is the major concern in this study, three different mesh sizes of 1.6, 1.2, and 0.8 mm are used for meshing the computational fluid domain. In each case of them, the other zones of the engine have the same mesh sizes. The engine geometry, dimensions, the initial filling pressure, the working fluid, the boundary and operating conditions are set according to the Stirling engine in [17] for comparison with the published experimental measurements. Properties of the working fluid (pressure, temperature and density) have periodic steady variations (steady cyclic variations). The model is executed till the variations in these properties between the first and last steps of the cycle are less than 1%. **Error! Reference source not found.** shows a comparison of the experimental [17] and the simulation of the p-v diagram at these different mesh sizes. It is clear that, mesh size of 0.8 mm achieves a reasonable agreement with the experimental measurements. At this mesh size, the engine produces work of 94 J/cycle while the experimental produces 90 J/cycle. Therefore, the error percentage is 4.5% which can be reasonably accepted.

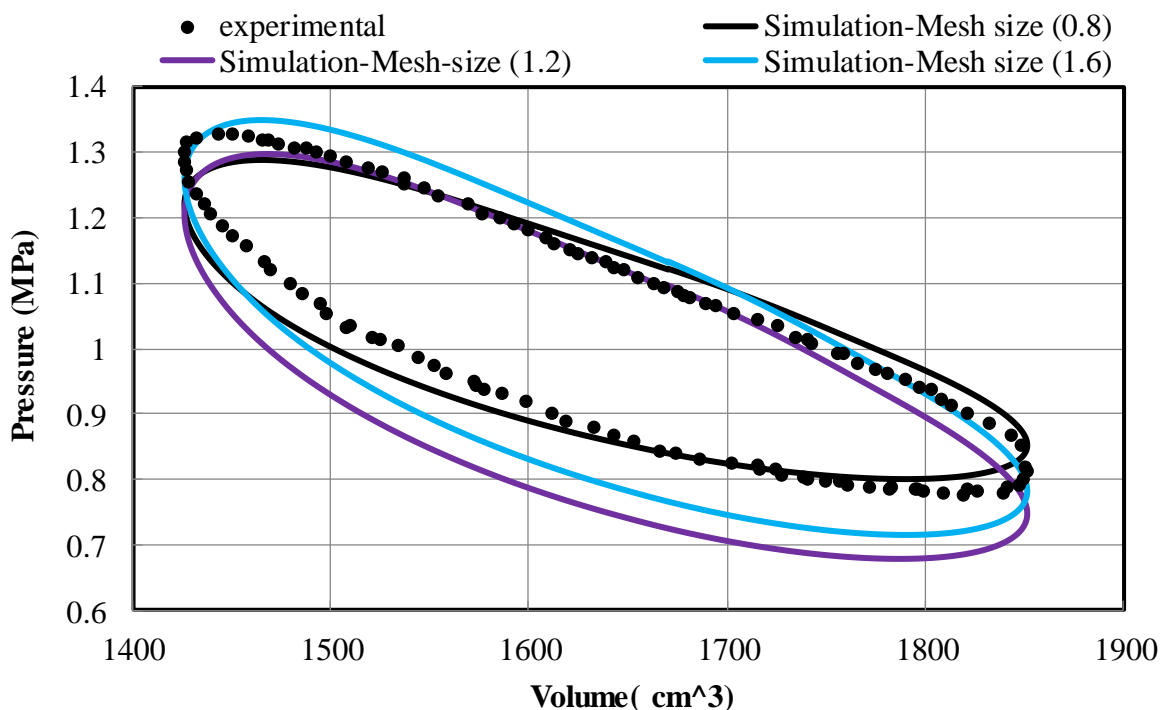


Fig. 4. p-v diagram at different mesh sizes verses experimental measurements

Figures 6 and 7 illustrates the meshing of all engine components and cross-sectional view of the meshed heater tubes.

3. Results and discussions

After constructing the five engine designs by gambit, each one of them is imported by ANSYS FLUENT-16 separately. The initial conditions, boundary conditions and working fluid properties are set and the pistons motion file is imported in ANSYS also. The SST k- ω is chosen. The time step of calculation is 0.0003333 seconds and solution convergence of each step is considered satisfied when the residuals of the velocity components, continuity, k and omega are 0.001 and the residual of energy equation is 1E-05. The model is executed

many engine cycles till the variations in the working fluid properties between the first and last steps of the cycle are less than 1%.

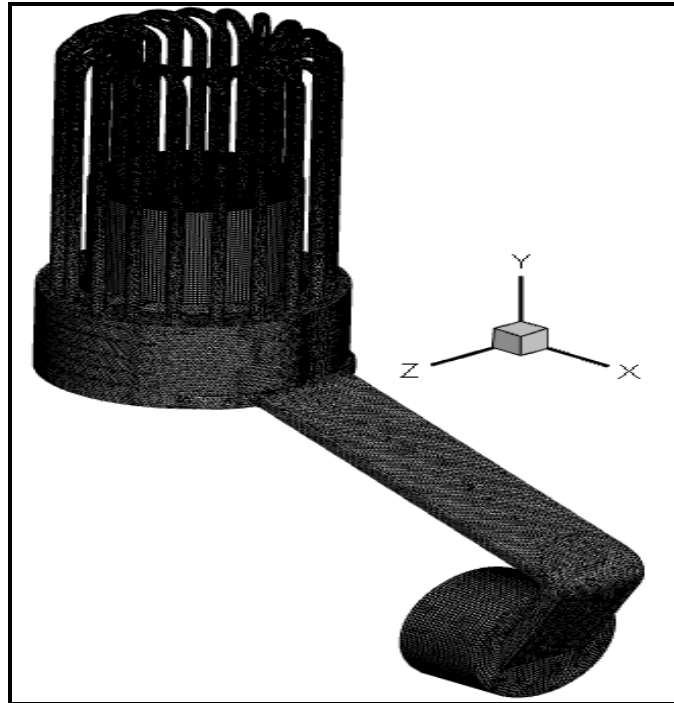


Fig. 6. 3D views the computational domain meshes

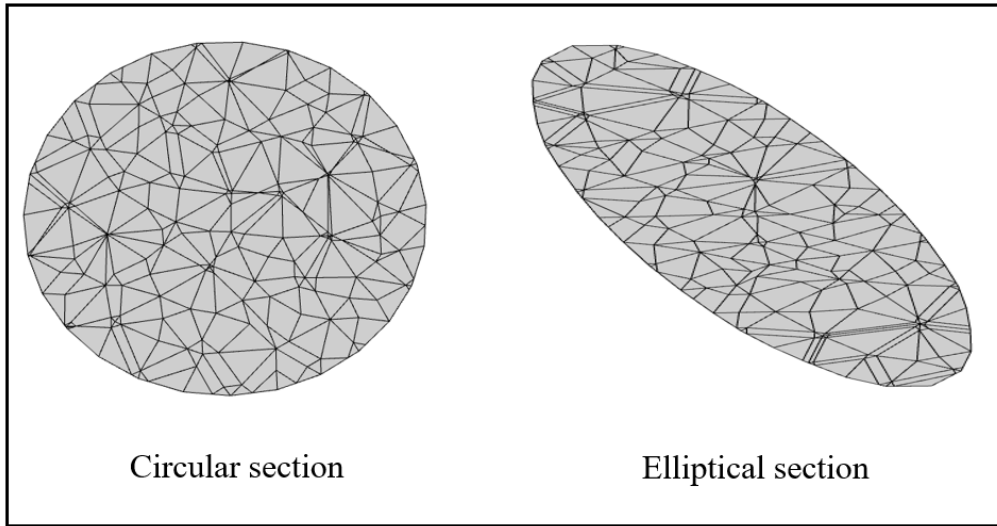


Fig. 7. Cross-sections of the meshed tubes

3.1. P-V diagram

The p-v diagram is important parameter of the engine as the integration of its area represents the output work. The p-v diagrams of the five heater designs are shown in Fig. 8. The circular section heater case produces the minimum area of the p-v diagram and the engine work is 139.48 J/cycle, while the elliptical section 2TR case produces the maximum area with output work of 149.91 J/cycle. Moreover, the elliptical sections with 4TR and 3TR produce p-v nearly conicoid under the 2TR case. By integration, their output works are 145.41 J/cycle and 147.04 J/cycle, respectively. The increments in the elliptical cases are due to the large surface of the heater tubes relative to the circular tube. But, twisting the elliptical tubes achieves little increments from 4TR to 2TR. However, these increments can be referred to the elongation of the gas path through the heater and the increase of tube surface area due to

twisting. The percentages of increments in output work are 4.3%, 5.4% and 7.4% for elliptical heater with 4TR, 3TR and 2TR, respectively, relative to the circular section heater.

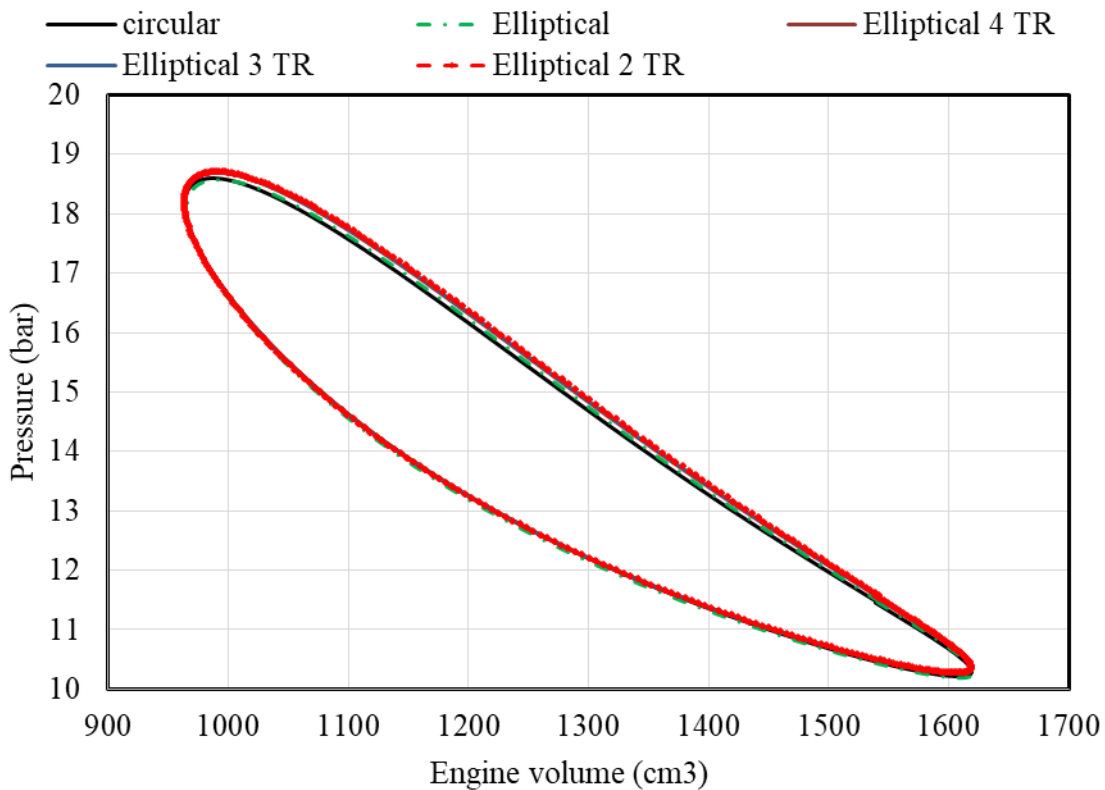


Fig. 8 p-v diagrams of the engine with the heater cases

3.2. Heat transfer through the heater

For understanding the heat transfer process through the heater tubes, the air motion through it will be explained through the engine cycle with the aid of Fig. 4. From 0° to 180° , the hot cylinder piston moves up blowing the air through the heater tubes, the regenerator, the cooler to the cold cylinder. Therefore, the air velocity (average velocity of the heater tube volume) is positive in this period as shown in Fig. 9. From 180° to 315° , the hot piston reverses its motion direction and moves down and the cold piston moves right which reverses the air motion through the heater tube. From 315° to 360° , the hot piston still moves down but the cold piston moves left resulting in volume expansion of the two cylinders, but the volume rate change of the cold cylinder is much bigger than that of the hot cylinder. Therefore, the air flows from the hot cylinder through to the heater the regenerator, the cooler then the cold cylinder. The average velocity values of the five designs are mainly the same as the five heater designs have the same cross section area, length and volume.

Reynolds number variations in Fig. 10 takes the same trend of the air velocity in Fig. 9 but Re of the circular section tube is bigger than that of the elliptical sections as the circular tube diameter is 6 mm but the elliptical tube hydraulic diameter is 4.9 mm.

Nusselt number in Fig. 11 is a function of the Re and the air velocity of the adjacent layer to the tube wall as the Prandtl number is taken constant, in this work, at average temperature value of $((900+300)/2=600$ K) to reduce the simulation run time. Therefore, it decreases rapidly in the period of 135° to 180° due to the decrement of air velocity. It has very low values in the period of 180° to about 210° although the air reverses its direction and starts to increase its velocity as shown in Fig. 9. This is because the adjacent layer velocity is very

low due to the opposite effects of the wall friction and its inertia from one side and the reversed air flow from the other side. Nusselt number of the circular section tube is bigger than that of the elliptical section tubes in Fig. 11 following the same behavior Re numbers in Fig 10.

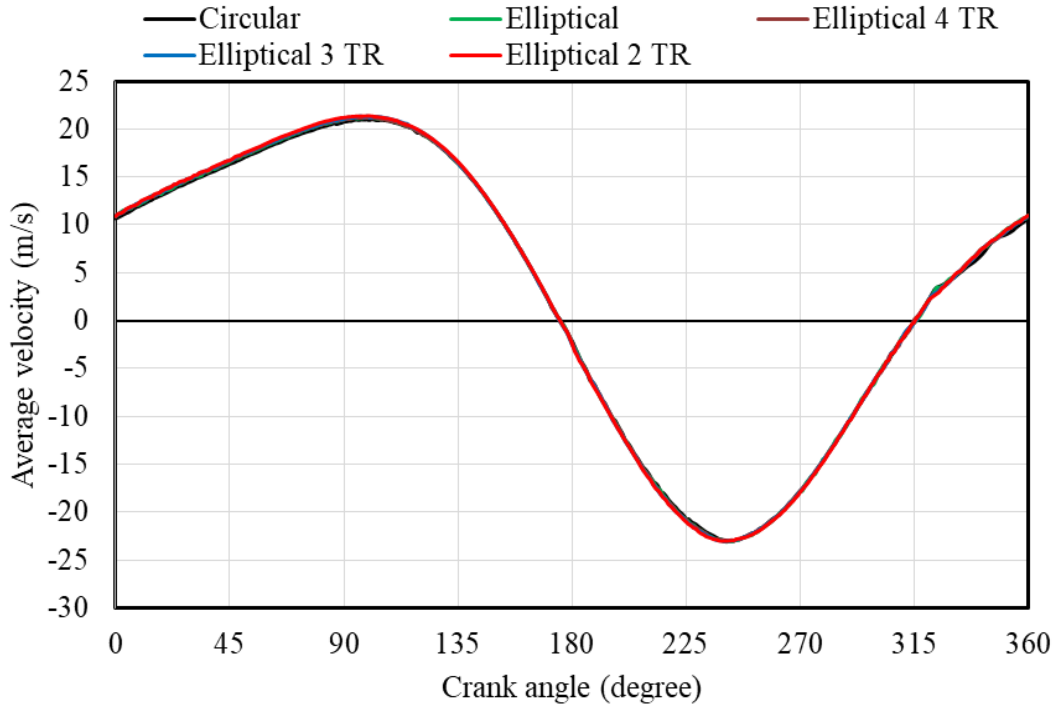


Fig. 9 Air velocity variations through one heater tube

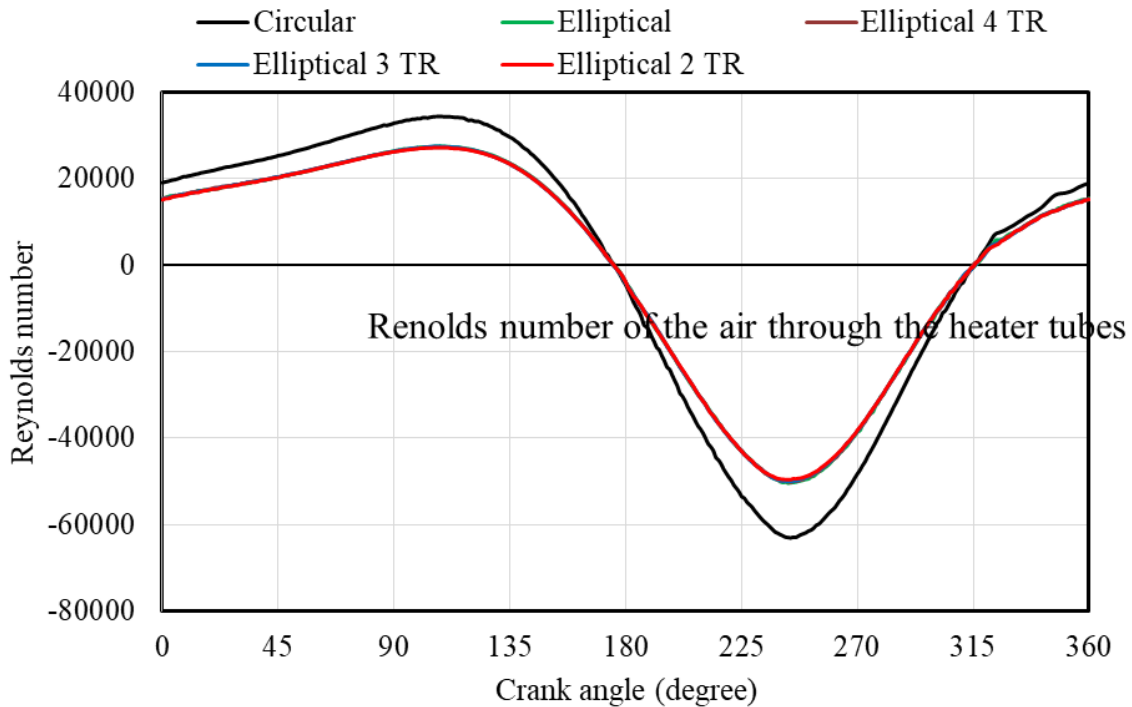


Fig. 10 Reynolds number variations through one heater tube

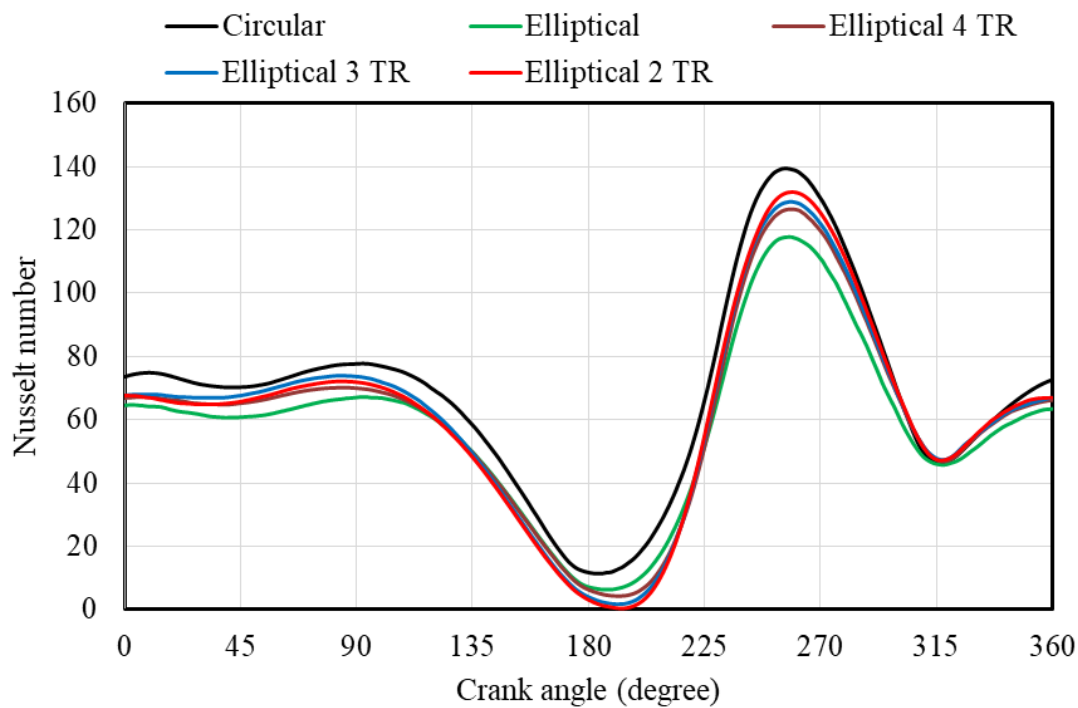


Fig. 11 Nusselt number variations through one heater tube

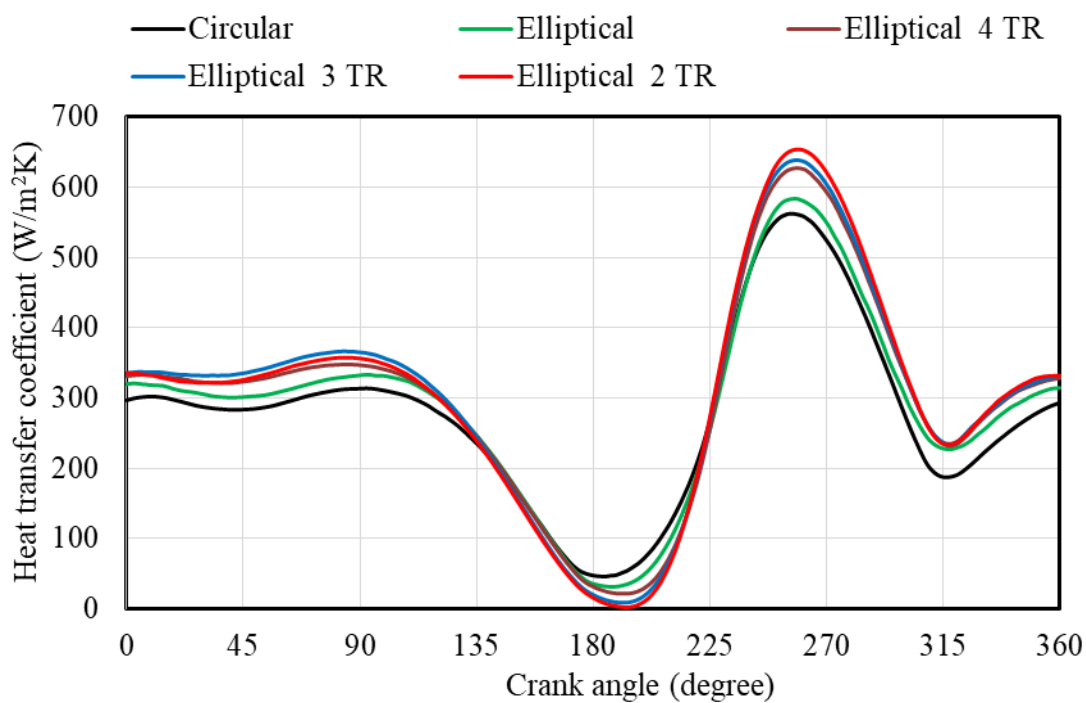


Fig. 12 Heat transfer coefficient in the heater tubes

Heat transfer coefficient is a function of Nu and the hydraulic diameter as the thermal conductivity of air is taken constant at average temperature value of 600 K. Heat transfer coefficient in Fig. 12 follows the same trend of Nusselt number in Fig. 11 but the heat transfer coefficient of the circular section tube is lower than that of the elliptical section tubes due to the decrement of the hydraulic diameter from 6 mm to 4.9 mm. Twisting the elliptical tubes cases a spiral motion of the air which increases the turbulence effect and hence the heat transfer coefficient. Increasing the twisting from 4TR to 2TR

results in considerable increment in heat transfer coefficient which enhance the heat transfer process through the heater tubes. The heater transfer rate in Fig. 13 follows the same trend of the heat transfer coefficient where it increases with using of elliptical tubes. Moreover, it increases with increasing the tube twisting from 4TR to 2TR due to the increase of tube surface area as shown in table 3.

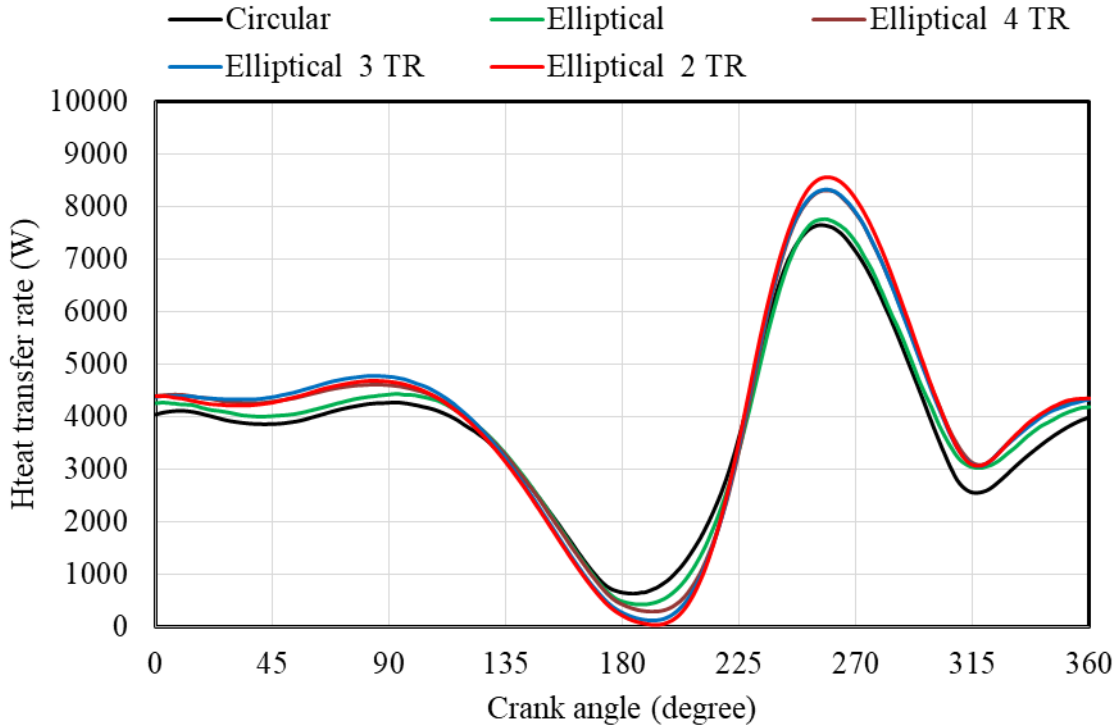


Fig. 13 Heat transfer rate through the heater walls

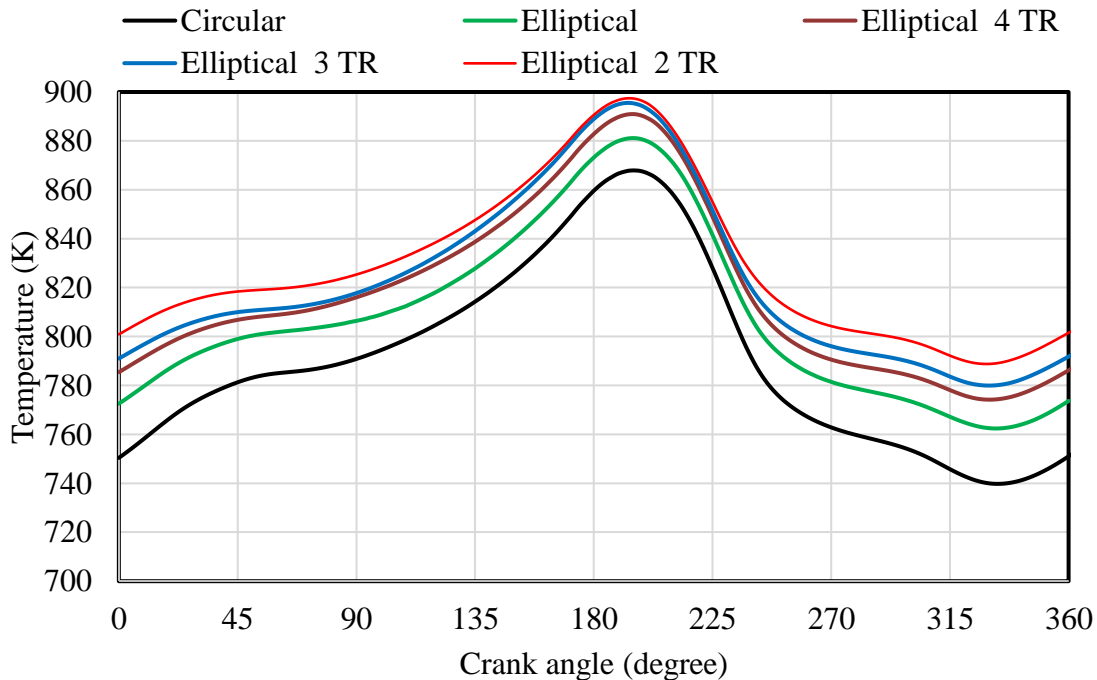


Fig. 5 Average air temperature in the heater tubes

The effect of heat transfer coefficient and heat transfer rates in Figs. 12 and 13 appears on the average air temperature through the heater tubes in Fig. 14. The air temperature

increases in the period from 0° to 180° as the air passes from the hot cylinder to the regenerator through the heater. At this period the circular cross section achieves the lowest level of temperature and the elliptical section 2TR achieves the highest.

3.3. Temperature contours

To illustrate the five heater designs effect on the temperature contours, section (A) in Fig. 4 which is 83 mm upper the hot cylinder is selected. The distance (83 mm) is long enough to reveal the design effect on the temperature distribution. The contours are illustrated at different crank angles to explain the designs effect through complete cycle. These angles are 60° , 120° , 180° , 240° , and 360° . Figure 15 illustrates these temperature contours. It can be noticed that the average temperature at any crank angle increases from circular section to elliptical 2RT. using ANSYS capabilities, the average temperatures through these sections are calculated. It is found that the maximum average temperature is achieved at 180° crank angle for the elliptical section, 2TR with a value of 882.29 K while the corresponding value of the circular section is 848.14 K. Therefore, an increment of 34.15 K is achieved.

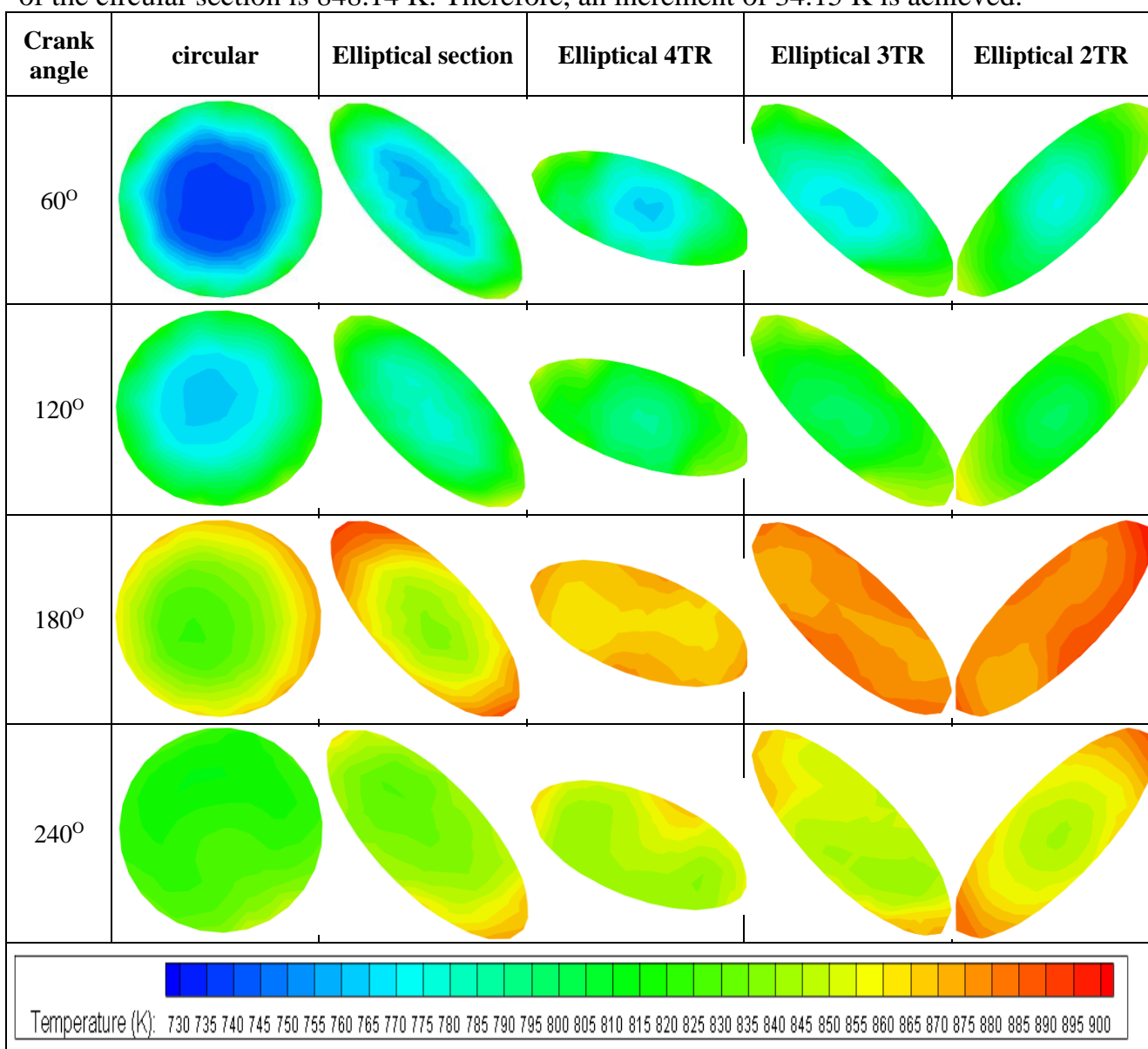


Fig. 65 Temperature contours at section A

3.4. Engine efficiency

Table 4. 4, illustrates the input, rejected energy rates and output power of the engine for the five designs. The input energy rates increase with using elliptical section tubes. Moreover, it increases with the increment of twisting from 4TR to 2TR. The input energy rate increases from 4018.74 W for circular section to 4227.84 W for elliptical 2TR section with a percentage increment of 5.2%. Also, the rejected energy rate increases from 2919.77 W to 2977.93 W for the same sections with a percentage increment of 1.4% due to the increment of the temperature level through the engine. The output power which is the difference between the input and rejected energy rates increases from 1162.36 W to 1249.26 for the same previous section with a percentage increment of 7.47%.

Table 4. Input and outputs energy rates

| Heater tubes | Input energy rate (W) | Rejected energy rate (W) | Output power (W) |
|----------------|-----------------------|--------------------------|------------------|
| Circular | 4081.74 | -2919.77 | 1162.36 |
| Elliptical | 4176.82 | -2959.69 | 1211.77 |
| Elliptical 4TR | 4227.84 | -2977.93 | 1249.26 |
| Elliptical 3TR | 4214.60 | -2982.95 | 1233.54 |
| Elliptical 2TR | 4245.87 | -3020.41 | 1225.34 |

Figure 16 illustrates the engine thermal efficiency of the five designs. The engine with circular section heater tubes achieves thermal efficiency of 28.48%. It increases with using elliptical section tubes to 29.55% for the Elliptical 2TR case. The corresponding percentage increment of the thermal efficiency is 3.76%.

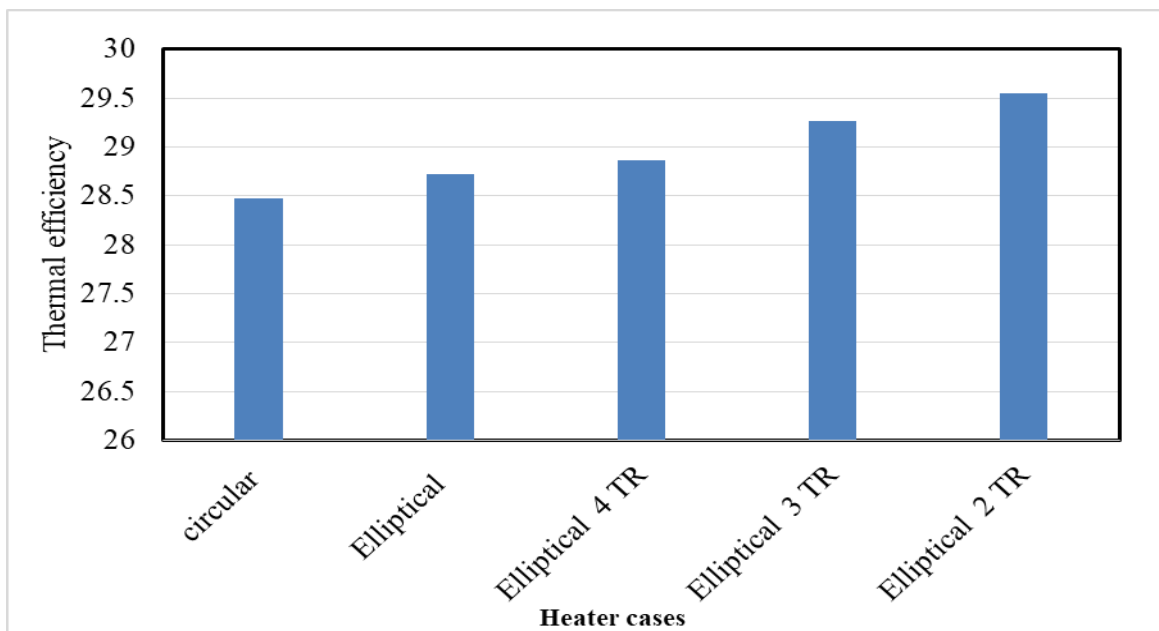


Fig. 16 Thermal efficiencies of the five cases

Table 5 illustrates the thermal efficiencies of the five studied cases besides the percentage increments relative to the circular heater tube.

Table 5. Thermal efficiency and percentage increment

| Heater tubes | Thermal efficiency (%) | Percentage increment (%) |
|----------------|------------------------|--------------------------|
| Circular | 28.47 | 0.0 |
| Elliptical | 28.72 | 0.87 |
| Elliptical 4TR | 28.86 | 1.34 |
| Elliptical 3TR | 29.27 | 2.78 |
| Elliptical 2TR | 29.55 | 3.76 |

4. Conclusions

This work examined the influence of different heater tube designs on the alpha Stirling engine performance. Circular section, elliptical section besides elliptical section with 4TR, 3TR, and 2TR are used. These different sections of the heater tube designs have the same cross-section area but they have different heat transfer areas. 3D engine model is constructed by Gambit program and the working fluid motion is solved by SST k- ω in ANSYS FLUENT-16. The main results can be concluded:

1. Using of heater tubes having elliptical twisted section increases the input energy rate and the output power.
2. The circular section heater tubes achieve the minimum input energy rate, output power and thermal efficiency with values of 4018.74 W, 1162.36 W and 28.47%, respectively.
3. The elliptical 2TR heater tubes achieve the maximum input energy rate, output power and thermal efficiency with values of 4245.87 W, 1225.34 W and 29.55%, respectively.
4. The percentage increments of input energy rate, output power and thermal efficiency are 5.2%, 7.47% and 3.76%, respectively for elliptical 2TR case.

Nomenclature

Symbols

| | |
|-------------|---|
| A_i | Interfacial area density, 1/m |
| \dot{C}_2 | Inertial resistance coefficient, 1/m |
| d_w | Wire diameter, m |
| D_h | Hydraulic diameter, m |
| h_i | Interspatial heat transfer coefficient, W/m ² .K |
| I | Turbulent intensity |
| K_f | Fluid phase thermal conductivity, W/m.k |
| K_s | Solid medium thermal conductivity, W/m.k |
| K_{eff} | Effective fluid thermal conductivity, W/m.k |
| L | Length of heater tube part, m |
| \dot{m} | Mass flow rate, kg/s |
| Nu_i | Inter-phase Nusselt number |
| P_i | Initial filling pressure, Pa |
| P_{atm} | Atmospheric pressure, Pa |
| R | Radius of curvature for heater tube part, m |

| | |
|----------------------|--|
| Re_i | Inter-phase Reynolds number |
| T_m | Mean temperature in Regenerator, K |
| u'_{max} | Maximum inlet flow velocity to porous media zone, m/s |
| (v_x, v_y, v_z) | Velocity component in Cartesian coordinates, m/s |
| (x_i, y_i, z_i) | The coordinates of cylinder centre, m |
| (x_o, y_o, z_o) | The coordinates of the air element centre, m |
| Greek symbols | |
| α | Permeability resistance coefficient, m ² |
| γ | Volumetric Porosity, % |
| μ_f | Flow dynamic viscosity, Pa. S |
| ρ_o | Density of air at atmospheric condition, kg/m ³ |
| ρ | Density of air at cylinder pressure. kg/m ³ |
| ρ_f | Flow density, kg/m ³ |
| ω_e | The engine angular speed, rpm |
| ω_s | The in-cylinder charge angular speed, rpm |

abbreviations

| | |
|-----|------------------------------|
| BDC | Bottom dead centre |
| CFD | Computational fluid dynamics |
| rpm | Revolution per Minute |
| TDC | Top dead centre |
| TR | Twist ratio |
| UDF | User Defined Function |
| 3D | Three dimensions |

References

- [1] D. Litalien *et al.*, “A low teperature Differential stirling engine foe power generation,” *Bifurcations*, vol. 45, no. 1. pp. 1–19, 2009, [Online]. Available: <http://dx.doi.org/10.1016/j.refiri.2017.07.010> <http://coop-ist.cirad.fr%0Ahttp://www.theses.fr/2014AIXM5048%0Ahttp://www.cairn.info/revue-management-et-avenir-2010-6-page-84.htm%0Ahttp://www.cairn.info/bifurcations--9782707156006-page-349.htm%0Ahttp://w>.
- [2] Z. Bao-sheng, C. Ning, and S. Zheng-chang, “New technology for coalbed methane power generation based on Stirling engine driven by porous burner,” *Procedia Earth and Planetary Science*, vol. 1, no. 1. pp. 1480–1483, 2009, doi: 10.1016/j.proeps.2009.09.228.
- [3] C. H. Cheng and Y. J. Yu, “Numerical model for predicting thermodynamic cycle and thermal efficiency of a beta-type Stirling engine with rhombic-drive mechanism,” *Renewable Energy*, vol. 35, no. 11. pp. 2590–2601, 2010, doi: 10.1016/j.renene.2010.04.002.
- [4] M. Tarawneh, F. Al-Ghathian, M. A. Nawafleh, and N. Al-Kloub, “Numerical Simulation and Performance Evaluation of Stirling Engine Cycle,” *Jordan Journal of Mechanical and Industrial Engineering*, Vol. 4, November 2010.
- [5] M. H. Ahmadi, M. A. Ahmadi, M. Mehrpooya, and M. A. Rosen, “Using GMDH neural networks to model the power and torque of a stirling engine,” *Sustainability (Switzerland)*, vol. 7, no. 2. pp. 2243–2255, 2015, doi: 10.3390/su7022243.
- [6] A. Chmielewski, S. Radkowski, R. Gumiński, and P. Szulim, “Experimental research and application possibilities of microcogeneration system with Stirling engine,” *Experimental research and application possibilities of microcogeneration system with Stirling engine*, vol. 95, no. 1. pp. 14–22, 2015.
- [7] B. Hoegel, “Thermodynamics-Based Design of Stirling Engines For Low-Temperature Heat Sources” Ph.D. thesis, Mech. Dep., University of Canterbury, New Zealand, 2014.
- [8] C. Alvarez-Herrera, A. R. Moreno-Nieto, and J. G. Murillo-Ramírez, “Study of temperature

- distribution over a Stirling engine by using the schlieren technique," Emerging Challenges for Experimental Mechanics in Energy and Environmental Applications, Proceedings of the 5th International Symposium on Experimental Mechanics and 9th Symposium on Optics in Industry (ISEM-SOI),2015, DOI centre 10.1007/978-3-319-28513-9.
- [9] Ke Li et al., "Analysis of Stirling engine heater head with liquid NaK for heat transportation," Research Gate, 2012, [Online]. Available: <https://www.researchgate.net/publication/291299162>.
- [10] H. Karabulut, H. Solmaz, and F. Aksoy, "A numerical study for Stirling engine heater development," Heat Transf. Res., vol. 48, no. 6, pp. 477–498, 2017, doi: 10.1615/HeatTransRes.2016011033.
- [11] D. Thombare, S. P. Kumbhar, D. G. Thombare, and N. K. Chhapkhane, "CFD Simulation of Stirling Engine Heater," International Journal of Engineering & Science Research, vol. 3, pp. 3077–3084, 2013, [Online]. Available: www.ijesr.org.
- [12] T. Akazawa, K. Hirata, T. Hoshino, H. Kita, and K. Fujiwara, "Design of Ceramics Heater for Stirling Engine," *Icdes*. 2014.
- [13] K. Kumar and B. T. Kuzhivel, "Parametric investigation of the hybrid regenerator of a Stirling cryocooler." Indian Journal of Cryogenics, vol. 41, pp. 81-85, (2016).
- [14] S. K. Andersen, H. Carlsen, and P. G. Thomsen, "Numerical study on optimal Stirling engine regenerator matrix designs taking into account the effects of matrix temperature oscillations," Energy Convers. Manag., vol. 47, no. 7–8, pp. 894–908, May 2006, doi: 10.1016/j.enconman.2005.06.006.
- [15] R. Gheith, F. Aloui, and S. Ben Nasrallah, "Study of the regenerator constituting material influence on a gamma type Stirling engine," J. Mech. Sci. Technol., vol. 26, no. 4, pp. 1251–1255, Apr. 2012, DOI: 10.1007/s12206-012-0218-9.
- [16] C. P. Speer, D. A. Miller, C. J. A. Stumpf, J. P. Michaud, and D. S. Nobes, "Modification of an ST05G-CNC stirling engine to use a low temperature heat source," *15th International Energy Conversion Engineering Conference, 2017*. 2017, doi: 10.2514/6.2017-4793.
- [17] S. Alfarawi, R. AL-Dadah, and S. Mahmoud, "Influence of phase angle and dead volume on gamma-type Stirling engine power using CFD simulation," Energy Convers. Manag. 124, pp. 130–140, 2016.
- [18] M. A. Mohammadi, A. Jafarian "CFD simulation to investigate hydrodynamics of oscillating flow in a Beta-type Stirling engine", Energy, Volume 153, 15 June 2018, Pages 287-300, [Doi.org/10.1016/j.energy.2018.04.017](https://doi.org/10.1016/j.energy.2018.04.017) .
- [19] L. Kuban, J. Stempka, A. Tyliszczak, "A 3D-CFD study of a γ -type Stirling engine", Energy, Volume 169, 15 February 2019, Pages 142-159, doi.org/10.1016/j.energy.2018.12.009 .
- [20] Wandong Zhao, Ruijie Li, Hailing Li, Ying Zhang, Songgang Qiu, "Numerical analysis of fluid dynamics and thermodynamics in a Stirling engine", Applied Thermal Engineering, 189 (2021) 116727, [Doi.org/10.1016/j.applthermaleng.2021.116727](https://doi.org/10.1016/j.applthermaleng.2021.116727).
- [21] ANSYS FLUENT User's Guide, chapter 7: Porous Media Conditions, Release 16.0 © ANSYS, Inc. January 2015
- [22] S.C. Costa, I. Barrino, M. Tutar, J.A. Esnaola, H. Barrutia, "The thermal non-equilibrium porous media modeling for CFD study of woven wire matrix of a Stirling regenerator, "Energy Convers. Manage. 89 PP. 473–483, 2015.

تأثير استخدام أنابيب السخان المستقيمة والمليوحة ذات المقطع البيضاوي على أداء محرك ستirlنج

الملخص:

تعتبر المساحة المعرضة لانتقال الحرارة خلال أنابيب السخان عاملًا مهمًا يؤثر تأثيراً عميقاً على قدرة المحرك والكفاءة الحرارية لمحركات "ستيرلنج". يعتبر محرك ستيرلنج من النوع "ألفا" هو محور اهتمامنا في هذه الدراسة. وفي تلك الدراسة، يتم استخدام أنابيب سخان ذات مقطع دائري بالإضافة إلى أنابيب بيضاوية المقطع مستقيمة وأخرى مليوحة بنسب التواء مختلفة. في هذه الدراسة تم استخدام ثلاث نسب التواء مختلفة وهم (اثنان، ثلاثة، أربعة) لأنابيب السخان بيضاوية المقطع. تمت المحاكاة عن طريق استخدام نموذج ثلثي الأبعاد لمحرك "ستيرلنج" باستخدام نموذج اضطراب $k-\omega$ من خلال SST k- ω استخدما

م برنامج أنسيز فلوونت نسخة رقم 16 وذلك لمحاكاة تدفق الهواء خلال الأسطوانة الساخنة ومنها إلى أنابيب السخان ثم المبادل الحراري ثم المبرد ثم إلى الأسطوانة الباردة بمحرك "ستيرلنج"، وكل ذلك يكون خلال دورة كاملة من عمل المحرك. أظهرت النتائج أن أنابيب المقطع البيضاوي أفضل من أنابيب المقطع الدائري. تم تحقيق الحد الأقصى لمعدل الطاقة الداخلة الشغل الناتج والكفاءة الحرارية باستخدام مقطع بيضاوي مع نسبة التفاف 2. هذه القيم هي ٤٢٤٥,٨٧ واط و ١٢٢٥,٣٤ واط و ٢٩,٥٥٪ على التوالي بزيادات نسبية مقدارها ٥,٢٪ و ٧,٤٪ و ٣,٧٪ على التوالي. بالنسبة لأنابيب السخان ذات المقطع الدائري.